Chinese Journal of Natural Medicines 24 (2026) 1015-1024

Contents lists available at ScienceDirect

Chinese Journal of Natural Medicines

journal homepage: www.cjnmcpu.com/

Original article

Aspergillines E–L with TDPs inhibitory and combined anti-tumor activities from marine fungus *Aspergillus* sp. EGF 15-0-3 as environmental-induced products

Xia Wei[a,b,Δ], Lishuang Guo[d,Δ], Xuewei Duan[a], Zekun Zhang[a], Linkun An[d,*], Juncheng Su[c,*], Cuixian Zhang[a,*]

[a] *School of Pharmaceutical Sciences, Guangzhou University of Chinese Medicine, Guangzhou 510006, China*
[b] *Guangxi Key Laboratory of Bioactive Molecules Research and Evaluation, School of Pharmaceutical Sciences, Guangxi Medical University, Nanning 530021, China*
[c] *State Key Laboratory for Chemistry and Molecular Engineering of Medicinal Resources, School of Chemistry and Pharmaceutical Sciences, Guangxi Normal University, Guilin 541004, China*
[d] *School of Pharmaceutical Sciences, Sun Yat-Sen University, Guangzhou 510006, China*

ARTICLE INFO

Article history:
Received 11 September 2025
Revised 1 December 2025
Accepted 22 February 2026
Available online 20 August 2026

Keywords:
Environmental-induced products
TDPs inhibitory activities
Combined anti-tumor activities
Marine fungus
Aspergillus sp. EGF 15-0-3

ABSTRACT

Systematical screening of the metabolic profile of marine fungus *Aspergillus* sp. EGF 15-0-3 using OSMAC-GNPS molecular networking cascade followed by target isolation of the environmental-induced products resulted the identification of eight unprecedented indole diketopiperazine-based hybrids (**1**–**8**) featuring three distinct chemical backbones. The structures of the obtained compounds were established by combination of extensive spectroscopic analyses, X-ray crystallography, and ECD calculations. All these environmental-induced metabolites were demonstrated to be unusual tyrosyl-DNA phosphodiesterase 2 inhibitors. Compound **3**, as the most outstanding example, showed selective synergistic antitumor effect when combined with the chemotherapeutic drugs.

1. Introduction

Topoisomerases (TOP) inhibitors, like etoposide (ETP) and camptothecin (CPT), are widely used in the treatment of systemic malignancies and solid tumors [1, 2]. However, the emergence of drug resistance often leads to therapeutic failure, with multiple underlying mechanisms contributing to this phenomenon. Among these, the upregulation of DNA repair enzymes is the major [3, 4]. Tyrosyl-DNA phosphodiesterases (TDPs), comprising TDP1 and TDP2, represent the principal enzymatic system for repairing DNA damage. While TDP1 has been extensively characterized in DNA repair mechanisms, as a protein identified merely in 2000, TDP2 represents a relatively unexplored therapeutic target [5]. To date, only seven distinct chemotypes have been identified as TDP2 inhibitors and no candidate has been progressed to preclinical or clinical testing [6]. TDP2 plays a pivotal role in tumor resistance to TOP inhibitors by catalyzing the repair of topoisomerase-mediated DNA lesions [7, 8]. Beyond its enzymatic functions, TDP2 serves as a critical factor in DNA damage repair by repairing TOP-induced DNA damage [9, 10]. Given the pivotal role of TDP2 in conferring tumor chemoresistance, innovative chemical scaffolds demonstrating both high TDP2 inhibitory potency and optimal drug-like characteristics are desired.

Marine organisms have yielded a diverse array of natural products with structural diversity and superior drug-like properties [11]. Since 1969, 18 marine-derived drugs have been approved, mainly for cancer therapy, while around 40 compounds are in clinical trials (https://www.marinepharmacology.org) [12, 13]. This is attributed to the unique characteristics of marine habitats [14]. Marine fungi, as key ecosystem components, exhibit remarkable adaptability through gene cluster regulation, leading to altered metabolic profiles [15-17]. Their high metabolic potential and ease of manipulation make them promising sources for novel drug discovery [18, 19].

Our research group has long interest in discovering bioactive chemical ingredients from marine fungi [20-23]. During our previous investigation, we have systematically screened the eighteen different culture conditions of the title fungus by using combination strategy of OSMAC-GNPS molecular networking cascade. Intriguingly, although the indole diketopiperazine alkaloid monomers were produced in ten out of eighteen tested media, metabolites with *m/z* ranging from 600 to 800 Da were solely found in the rice medium among the ten monomers identified tested media, indicating the presence of unusual environmental-induced metabolites in rice medium. The subsequent chromatographic approaches resulted in the discovery of four novel cytotoxic indole diketopiperazine-based hybrids [24]. As a part of our continuous study on the title fungus, we paid particular note to the presence of an array of environmental-induced products with similar molecular weight but distinct MS fragments in the rest chromatographic fractions (Fig. S1). Motivated by these revelations, we enlarged the fermentation scale of this strain on the rice medium, and subsequently targeted isolation resulting eight new indole

* Corresponding author.
E-mail addresses: lssalk@mail.sysu.edu.cn (L. An); su_juncheng@163.com (J. Su); zhangcuixian@gzucm.edu.cn (C. Zhang)
Δ These authors contributed equally to this work.

https://doi.org/10.1016/S1875-5364(26)61199-5

diketopiperazine-based hybrids (**1**–**8**) featuring three types of unusual skeletons as environmental-induced products (Fig. 1). Structurally, aspergillines E–I (**1**–**5**) possess a highly functionalized 6/6/5/6/6 pentacyclic scaffold with a pyrano[3′,2′:7,8]isochromeno [4,3-*b*]pyrazino[2,1-*i*] indole backbone, aspergilline J (**6**) bear a spiro[piperazine-2,2′-pyrano[3,4,5-*de*]chromene core, and aspergillines K (**7**) and L (**8**) represent the first benzaldehyde-based indole alkaloids with unprecedented backbones. Interestingly, instead of showing direct growth inhibition to cancer cells, these compounds showed significant synergistic effect when combined with the chemotherapeutic drugs *via* inhibition of tyrosyl-DNA phosphodiesterase 2 (TDP2). Herein we outline their isolation, structure elucidation, and biological evaluation.

2. Results and discussion

Aspergilline E (**1**) was obtained as a rufous powder with a molecular formula of $C_{39}H_{41}N_3O_6$ based on its HR-ESI-MS ion at *m/z* 648.3073 $[M + H]^+$ (Calcd. for $C_{39}H_{42}N_3O_6$ 648.3074), indicating 21 degrees of unsaturation. The UV spectrum displayed absorption maxima at 226, 269, and 339 nm. The IR spectrum suggested the presence of amine (3354 and 2966 cm^{-1}), carbonyl (1685, 1660, and 1654 cm^{-1}) as well as benzene ring (1608, 1473 and 1456 cm^{-1}). A detail analysis of the ^1H and ^{13}C NMR spectra of **1** suggested the presence of one paraquinone group, two amide carbonyls, two trisubstituted double bonds, one *cis*-disubstituted double bond, one monosubstituted double bond, a 2,3-disubstituted indole moiety, two quaternary carbons, five methines, two methylenes, and six methyls (including one methoxy). Comprehensive analysis of 1D and 2D NMR data of **1** resulted in the full assignment of the proton signals to their respective carbons (Table 1).

Interpretation of the ^1H–^1H COSY spectrum of **1** allowed the establishment of four spin-coupling systems (Fig. 2). In the HMBC spectrum, correlations from NH-1 to C-3/C-3a/C-15, from H-4 to C-3/C-7a, from H-7 to C-3a, from H-8 to C-3a/C-10, from NH-14 to C-8/C-10/C-12, from H-17 to C-15, H_3-18/H_3-19 to C-2, as well as from H-20 to C-13, suggested the existence of an indole diketopiperazine unit (unit A, Fig. 2). In addition, the ^1H–^1H COSY correlations of H-7′/H-8′/H-9′/H-10′/H-11′/H-12′/H_3-13′/H-20 and H-15′/H-16′, in conjunction with the key HMBC correlations from H-4′ to C-2′/C-6′, H-7′ to C-1′/C-5′, H-14′ to C-2′/C-8′, H-15′ to C-2′/C-4′, H-16′ to C-18′/C-19′, as well as H-20′ to C-14′, allowing the addition signals to be presumed as an quinoid polyketide unit (unit B, Fig. 2).

The assembly of unit A and unit B *via* C-20–C-12′, C-12–C-9′, and N-11–C-7′ bonds were deduced from the HMBC correlations from H-12′ to C-12, H-9′ to C-13, and H-7′ to C-10, respectively. Therefore, the planar structure of **1** was determined as being representative of a novel class of indole diketopiperazine hybrids possessing a highly functionalized 6/6/5/6/6 pentacyclic scaffold with a complex isochromeno[4,3-*b*]pyrazino[2,1-*i*]indole backbone. The relative configuration of **1** (Fig. 3) was established by comprehensive analysis of the NOESY spectrum of **1** along with comparison with that of aspergilline A [24], which was confirmed by X-ray.

Aspergilline F (**2**) was obtained as a rufous powder. The HR-ESI-MS ion peaks at *m/z* 648.3074 $[M + H]^+$ (Calcd. for $C_{39}H_{42}N_3O_6$ 648.3074) observed of **2** showed that it has the same molecular formula as **1**. Further comprehensive analysis of the 1D (Table 1) and 2D (Figs. 2 and 3) NMR spectra of **2** revealed the NMR data of **2** were highly resembled with those of **1**, except for the differences of the resonances assigned to C-10 [δ_C = 158.1 (**2**), 161.9 (**1**)], C-13 [δ_C = 167.2 (**2**), 168.4 (**1**)], C-7′ [δ_C = 47.8 (**2**), 49.5 (**1**)], C-8′ [δ_C = 72.4 (**2**), 69.1 (**1**)], and C-9′ [δ_C = 46.4 (**2**), 42.2 (**1**)]. Moreover, the distinct NOESY correlations of H-20a and H_3-13′, indicated that H-20a and H_3-13′ were cofacial and situated in the *α*-orientation. NOESY correlations of H-20b and H-7′/H-9′, as well as H-9′ and H-8′/H_3-20′, suggested H-20b, H-7′, H-8′, H-9′and H_3-20′ were in the *β*-orientation. Meanwhile, the double bond at C-8 was *Z*-geometry could be deduced by the NOESY correlations of H-4 and NH-14 (Fig. 3), indicate compound **2** was the C-12 epimer of **1**.

The molecular formula of aspergilline G (**3**) was $C_{38}H_{39}N_3O_6$ based on its HR-ESI-MS ion at *m/z* 634.2899 $[M + H]^+$ (Calcd. for $C_{38}H_{40}N_3O_6$ 634.2917). Compared to **2**, the loss of 14 mass units in the HR-ESI-MS data and disappearance of the methoxy group, as well as the appearance of the hydroxy group in the 1D NMR spectra (Table 1) indicated that **3** was the demethylated derivative of **2**, which was confirmed by the HMBC correlations (Fig. 2). Meanwhile, similar NOESY correlations corroborated the structure of **3** (Fig. 3).

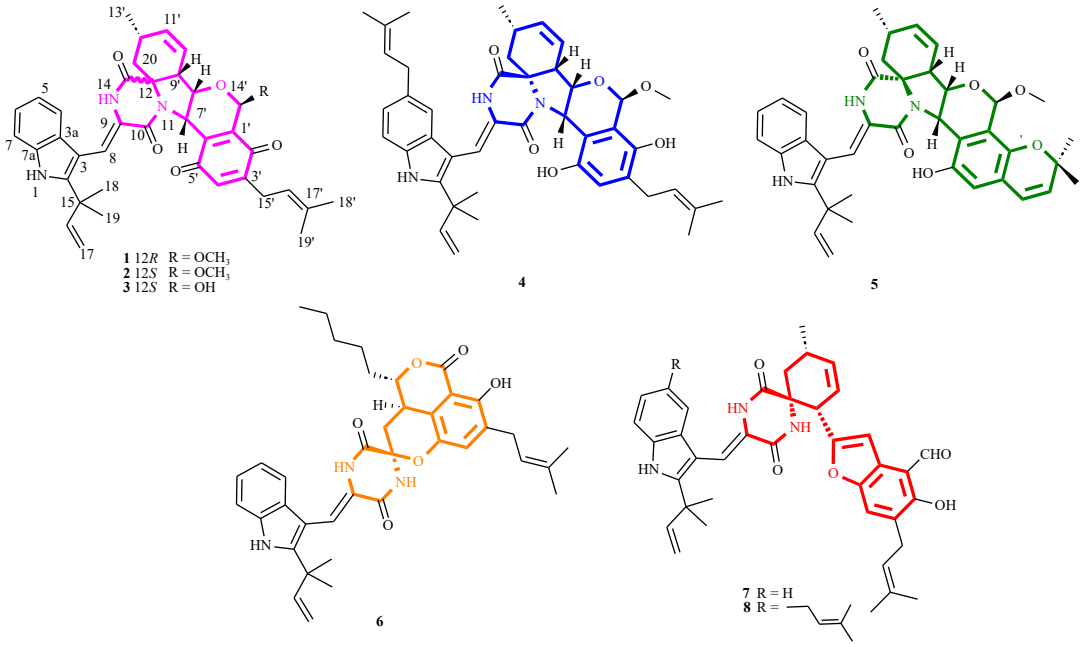

Fig. 1 Chemical structures of compounds **1**–**8**.

Table 1 ^{1}H NMR (400 MHz) and ^{13}C NMR (100 MHz) data of **1**–**3** in DMSO-d_6 (J in Hz)[a].

No.	1		2		3	
	δ_H (J, Hz)	δ_C, type	δ_H (J, Hz)	δ_C, type	δ_H (J, Hz)	δ_C, type
1	11.09 (s)		11.06 (s)		11.05 (s)	
2		145.2, C		144.6, C		144.6, C
3		104.4, C		103.4, C		103.8, C
3a		126.3, C		126.2, C		126.2, C
4	7.15 (d, 7.8)	118.9, CH	7.14 (d, 7.8)	118.9, CH	7.13 (d, 7.8)	118.9, CH
5	6.97 (t, 7.6)	119.2, CH	7.01 (t, 7.8)	119.4, CH	7.02 (t, 7.8)	119.4, CH
6	7.08 (t, 7.6)	120.7, CH	7.08 (t, 7.8)	120.7, CH	7.09 (t, 7.8)	120.7, CH
7	7.43 (d, 7.8)	111.8, CH	7.42 (d, 7.8)	111.7, CH	7.42 (d, 7.8)	111.7, CH
7a		135.0, C		134.7, C		136.3, C
8	6.91 (s)	113.8, CH	6.82 (s)	113.0, CH	6.82 (s)	112.8, CH
9		125.2, C		124.1, C		124.2, C
10		161.9, C		158.1, C		158.0, C
11						
12		65.4, C		65.6, C		65.6, C
13		168.4, C		167.2, C		167.2, C
14	9.47 (s)		9.42 (s)		9.41 (s)	
15		39.3, C		39.3, C		39.3, C
16	6.06 (dd, 17.6, 10.8)	145.1, CH	6.04 (dd, 17.2, 10.4)	145.2, CH	6.05 (dd, 17.2, 10.4)	145.2, CH
17	a 5.01 (m)	112.0, CH_2	a 4.98 (m)	111.9, CH_2	a 5.03 (m)	111.8, CH_2
	b 5.04 (m)		b 5.02 (m)		b 5.00 (m)	
18	1.49 (s)	27.7, CH_3	1.46 (s)	27.7, CH_3	1.46 (s)	27.6, CH_3
19	1.45 (s)	28.0, CH_3	1.41 (s)	28.0, CH_3	1.42 (s)	28.0, CH_3
20	a 1.90 (m)	38.4, CH_2	a 1.65 (m)	38.3, CH_2	a 1.64 (m)	38.2, CH_2
	b 2.30 (m)		b 2.17 (m)		b 2.14 (m)	
1′		147.4, C		147.7, C		147.7, C
2′		184.0, C		184.1, C		184.4, C
3′		138.2, C		137.1, C		137.0, C
4′	6.78 (br s)	132.8, CH	6.76 (s)	132.7, CH	6.75 (s)	132.6, CH
5′		184.6, C		184.5, C		184.8, C
6′		135.7, C		135.1, C		135.0, C
7′	4.77 (d, 2.6)	49.5, CH	4.54 (d, 2.6)	47.8, CH	4.52 (d, 2.8)	47.7, CH
8′	4.38 (t, 2.6)	69.1, CH	4.17 (d, 2.6)	72.4, CH	4.28 (d, 2.8)	71.8, CH
9′	3.29 (*br* s)	42.2, CH	3.15 (m)	46.4, CH	3.07 (m)	46.6, CH
10′	5.74 (m)[a]	121.9, CH	5.84 (m)[a]	124.3, CH	5.83 (m)[a]	124.3, CH
11′	5.75 (m)[a]	134.8, CH	5.82 (m)	135.2, CH	5.82 (m)[a]	135.2, CH
12′	2.27 (m)	28.1, CH	2.29 (m)	26.4, CH	2.28 (m)	26.5, CH
13′	1.06 (d, 6.8)	19.9, CH_3	1.12 (d, 7.0)	20.0, CH_3	1.12 (d, 7.0)	20.0, CH_3
14′	5.44 (s)	92.1, CH	5.39 (s)	92.9, CH	5.70 (d, 6.4)	85.6, CH
15′	3.10 (d, 7.2)	27.1, CH_2	3.12 (d, 7.2)	27.2, CH_2	3.10 (d, 7.2)	27.2, CH_2
16′	5.19 (t, 7.2)	119.1, CH	5.21 (t, 7.2)	118.8, CH	5.20 (t, 7.2)	118.9, CH
17′		135.1, C		135.1, C		135.1, C
18′	1.65 (s)	17.7, CH_3	1.65 (s)	17.7, CH_3	1.65 (s)	17.7, CH_3
19′	1.74 (s)	25.5, CH_3	1.73 (s)	25.5, CH_3	1.73 (s)	25.5, CH_3
20′	3.40 (s)	55.9, CH_3	3.45 (s)	56.2, CH_3		
14′-OH					7.15 (s)	

[a] Overlapped signals are reported without designating multiplicity.

Aspergilline H (**4**) was obtained as a lightly yellow powder, with a molecular formula of $C_{44}H_{51}N_3O_6$ based on its HR-ESI-MS ion at *m/z* 718.3846 $[M + H]^+$ (Calcd. for $C_{44}H_{52}N_3O_6$ 718.3856), indicating 21 degrees of unsaturation. A detail analysis of the 1D (Table 1) and 2D NMR data obtained for **4** with those of **1**, indicating the structural similarity of these two compounds. The significant differences were the appearance of a penta-substituted benzene ring signals [δ_H 6.62 (s); δ_C 115.7, 119.6, 123.0, 131.1, 145.2 and 150.2] in **4**, instead of the paraquinone group signals in **1**, and the additional of an isoprene group signals [δ_H 1.65 (s), 1.67 (s), 2.30 (m), 3.18 (m), and 5.26 (m); δ_C 17.8, 25.6, 28.0, 122.2, and 130.7], while an aromatic proton signal at δ_H 6.97 (t, 7.6, H-5) in **1** was absent in **4**, as evidenced by the observed HMBC correlations from H-21 to C-4/C-6, H-22 to C-5/C-24/C-25, H-4′ to C-2′/C-6′, H-7′ to C-1′/C-5′, H-14′ to C-2′, and H-15′ to C-2′/C-4′ (Fig. 2). Further ^{1}H–^{1}H COSY, HMBC and NOESY (Fig. 3) correlations allowed the complete assignment for **4**. Therefore, the gross structure of **4** was elucidated as shown in Fig. 1.

Aspergilline I (**5**) was obtained as a lightly yellow powder with a molecular formula identical to aspergilline A ($C_{39}H_{41}N_3O_6$) based on its HR-ESI-MS ion at *m/z* 648.3075 $[M + H]^+$ (Calcd. for $C_{39}H_{42}N_3O_6$ 648.3074). Extensive analysis of the 1D (Table 2) and 2D NMR data revealed **5** possesses the same planar structure as aspergilline A [24]. The major spectroscopic differences between **5** and aspergilline A could be attributed to C-10 [δ_C = 160.7 (**5**), 163.9 (aspergilline A)], C-12 [δ_C = 65.9 (**5**), 67.0 (aspergilline A)], C-7′ [δ_C = 51.4 (**5**), 54.6 (aspergilline A)], C-8′ [δ_C = 72.9 (**5**), 68.7 (aspergilline A)], as well as C-9′ [δ_C = 44.5 (**5**), 41.9 (aspergilline A)], which was further confirmed by the correlations in the HMBC spectrum (Fig. 2). In addition, the NOESY cross-peaks of H-7′/H-9′ and H-20a, as well as H-20a and H_3-13′, indicating **5** was the 12-epimer of aspergilline A (Fig. 3).

Aspergilline J (**6**) was obtained as a lightly yellow powder with the same molecular formula as that of aspergilline D [24] ($C_{38}H_{43}N_3O_6$) based on its HR-ESI-MS ion at *m/z* 638.3223 $[M + H]^+$ (Calcd. for $C_{38}H_{44}N_3O_6$ 638.3230). The ^{1}H and ^{13}C NMR data (Table 2) were found to be similar to those of aspergilline D. Further analyses of 2D NMR data confirmed that **6** and aspergilline D shared the identical planar structures (Fig. 2). The notably different signals observed were attributed the C-10, C-20, and C-7′, indicating these two compounds were epimers at C-12. This conclusion was verified subsequently by the observation of key NOESY correlations between NH-11 and H-20b, as well as H-20a and H-8′ (Fig. 3).

Aspergilline K (**7**) was obtained as a yellow powder, with a molecular formula of $C_{38}H_{39}N_3O_5$ based on its HR-ESI-MS ion at *m/z* 618.2964 $[M + H]^+$ (Calcd. for $C_{38}H_{40}N_3O_5$ 618.2968). Exhaustive analyses of the NMR data indicated **7** also possesses the typical indole diketopiperazine fragment (fragment A, Fig. 2). Except for the signals for these functional groups, the combined 1D NMR (Table 3) and HSQC spectra revealed the presence of an additional 19 carbons, including three methyls, one methylene, two methines, one pair of disubstituted double bond, two pairs of trisubstituted double bonds, one penta-substituted benzene ring, and an aldehyde group. The ^{1}H–^{1}H COSY correlations of H-9′/H-10′/H-11′/H-12′/H_3-13′/H-20 and H-15′/H-16′, in conjucted with the key HMBC correlations from H-4′ to C-2′/C-6′, H-7′ to C-1′/C-5′/C-9′, H-14′ to C-2′/C-6′, H-15′ to C-2′/C-4′, H_3-18′/H_3-19′ to C-16′, as well as 2′-OH to C-1′/C-3′, allowing the addition signal to be presumed as a benzaldehyde fragment containing a furan ring (fragment B, Fig. 2). The connection of fragments A and B *via* C-20–C-12′ and C-12–C-9′ bonds could be defined by the HMBC correlations between H-20 and C-13 as well as H-10′/H-12′ and C-12. Therefore, the planar structure of **7** could be established as a novel indole diketopiperazine-benzaldehyde hybrid.

In the NOESY spectrum, NOESY correlations of NH-11/H-20a

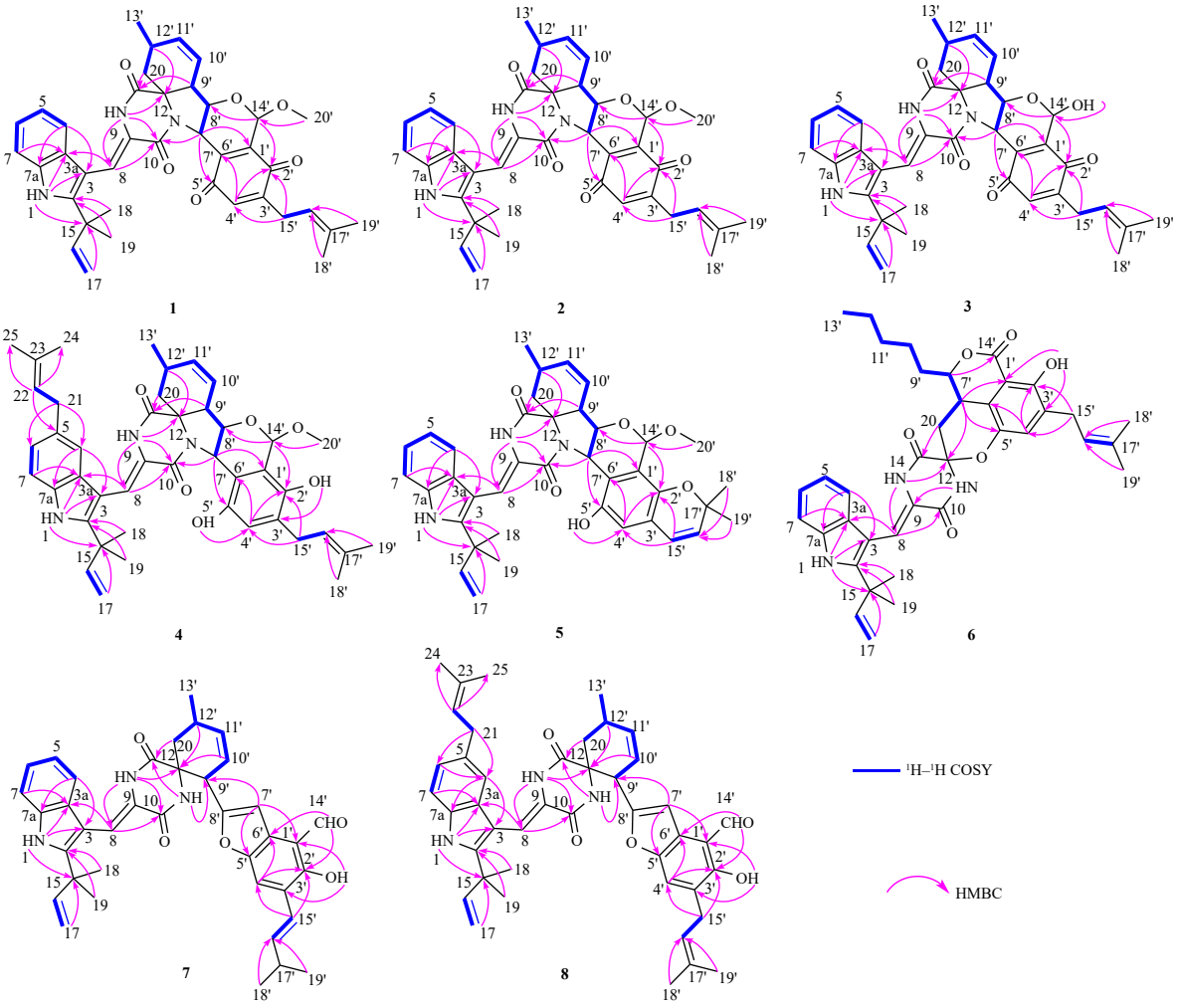

Fig. 2 ^{1}H–^{1}H COSY and key HMBC correlations of **1**–**8**.

and H-20a/H_3-13′ (Fig. 3) revealed these protons to be in a cofacial relationship. In addition, the NOE correlation observed for H-20b/H-9′, suggesting the relative configuration of **7** was established to be 12*R**,9′*S**,12′*S**. Moreover, a suitable crystal of **7** was obtained and firmly confirmed the planar structure and the relative configurations of **7** (Fig. 4, CCDC 2353833).

Aspergilline L (**8**) was obtained as a yellow powder, with a molecular formula of $C_{43}H_{47}N_3O_5$ based on its HR-ESI-MS ion at *m/z* 686.3588 $[M + H]^+$ (Calcd. for $C_{43}H_{48}N_3O_5$ 686.3594). Detailed analysis of 1D (Table 3) and 2D NMR data of **8** revealed that **8** was the C-5 prenylated analogue of **7**, the only difference was the presence of an additional isoprene group [δ_H 1.60 (s), 1.62 (s), 3.32 (d, 7.0), and 5.28 (dd, 7.0, 1.6); δ_C 17.6, 25.5, 34.3, 121.4, and 132.3] in **8**, which was supported by the HMBC correlations from H-21 to C-4/C-6, and H-22 to C-5/C-23/C-24 (Fig. 2).

It is intriguing to note that the specific rotations of compounds **1**–**8** were barely measurable, suggesting that they were all obtained as racemic mixtures. To determine their absolute configurations, chiral HPLC was employed to separate the racemic compounds **1**–**8** into their respective optically pure enantiomers, (+)-**1**, (−)-**1**, (+)-**2**, (−)-**2**, (+)-**3**, (−)-**3**, (+)-**4**, (−)-**4**, (+)-**5**, (−)-**5**, (+)-**6**, (−)-**6**, (+)-**7**, (−)-**7**, (+)-**8**, and (−)-**8**, respectively. Subsequently, the absolute configurations of these enantiomers were definitively established by ECD experiments with the assistance of quantum chemical calculations (Fig. 5, see the Supporting information for details).

Previously, we identified four cytotoxic environmental-induced indole diketopiperazine-based hybrids. Therefore, compounds **1**–**8** were initially evaluated for their cytotoxicities against a panel of cancer cells using CCK8 assay. However, none of these compounds exhibited any inhibitory effects.

Tyrosyl-DNA phosphodiesterase 2 (TDP2) is a critical enzyme involved in repairing DNA damage caused by TOP inhibitor [6]. Upregulation of TDP2 is considered as a defensive feedback of tumor cells in response to etoposide and other TOP inhibitors exposure and is the major causality of drug-resistance [25, 26]. While TDP2 inhibitors have shown promise for sensitizing cancer cells to TOP inhibitors, there is a limited number of chemotypes reported as TDP2 inhibitors, and no TDP2-targeting inhibitors have been approved for clinical use or entered the market.

Focusing on TDP2 inhibitors discovery, we evaluated the TDP2 inhibitory activities of isolated compounds **1**–**8**. While all compounds except **4** demonstrated potential activity, compounds **2** and **3** emerged as particularly promising candidates (Table 4).

Since **2** and **3** possessed remarkable potency against TDP2, we wonder whether their TDP2 inhibitory effects could be reflected in anti-tumor effects at the cellular level. To our surprise, although both **2** and **3** bear an identical chemical skeleton, and **2** was demonstrated to possess better TDP2 inhibitory potency, only **3**, with a 14′-OH, instead of its 14′-OCH_3 of analogue **2**, showed significant synergistic effect with the chemotherapeutic etoposide (ETP) or camptothecin (CPT) against the proliferation of DU-145, MHCC-97, A549, MDA-MB-231, and Hgc-27 cells (Fig. 6). These results indicated that **3** could serve as a promising leading compound for the further structural optimization, and the subsequent structure-activity relationship study may provide gainful insights for developing new TDP2 inhibitor.

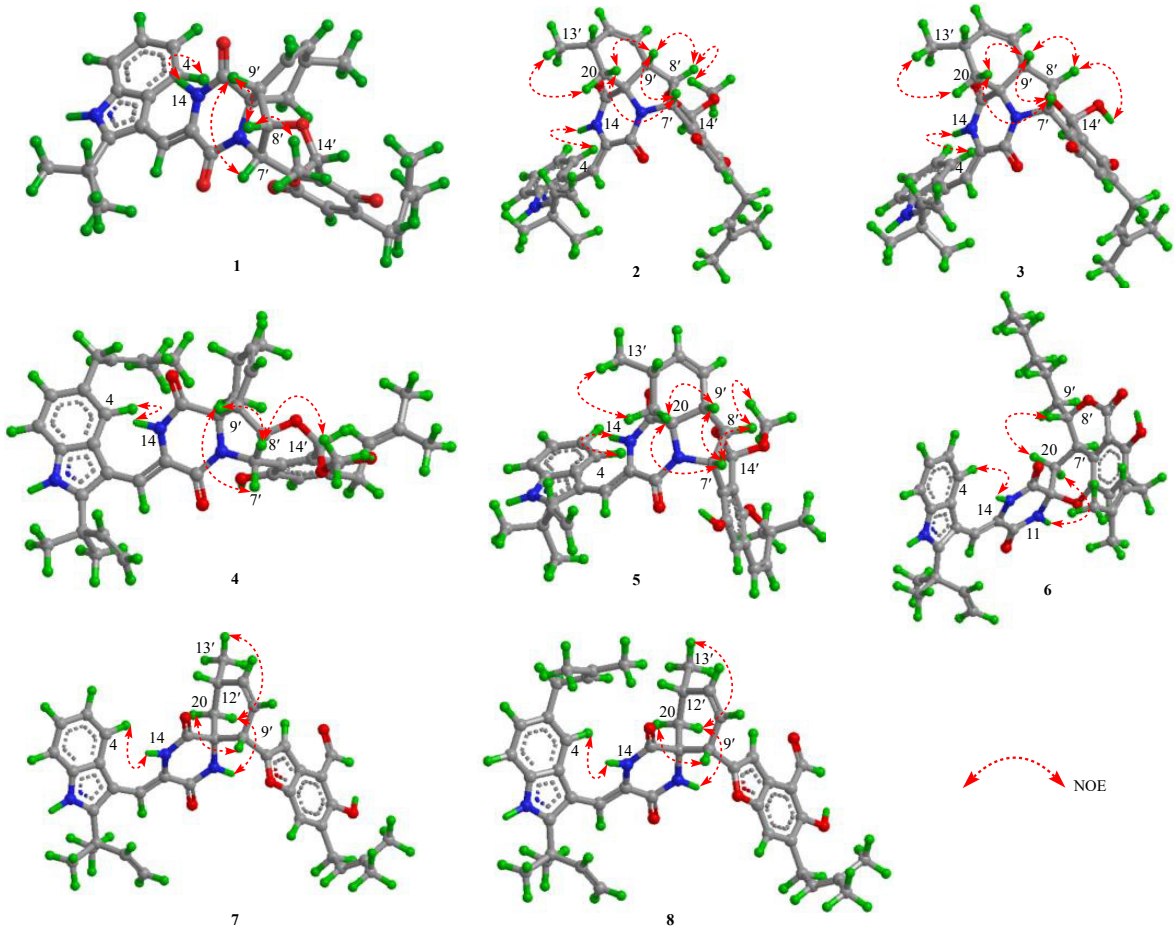

Fig. 3 Key NOE correlations of compounds **1**–**8**.

3. Conclusion

In summary, the discovery of eight novel environmental-induced products with three distinct structural scaffolds showcases the remarkable chemical diversity of marine fungi under varying environmental conditions, and enriches the structural diversity of indole-diketopiperazine derivatives. Importantly, these compounds have been demonstrated to act as TDP2 inhibitors. Notably, compound **3**, which stands out among the identified compounds, demonstrates a selective synergistic antitumor effect when used in combination with chemotherapeutic drugs, highlighting its potential as a novel therapeutic agent. The above findings enrich the chemical and biological diversity of TDP2 inhibitors.

4. Experimental

4.1. General experimental procedures

The general experimental procedures were performed as described previously [24].

4.2. Fungal strain and fermentation

Details of the collection site and taxonomic identification of the strains of *Aspergillus* sp. EGF 15-0-3 material have been reported in previous work [24]. The fungus *Aspergillus* sp. EGF 15-0-3 was activated on PDB medium under a rotatory shaker at 165 r·min^{-1} at 28 °C for 5 days to obtained the seed culture. Subsequently seed culture was subcultured in polished glutinousr rice medium (each 1 L containing 100.0 g of rice, 0.3% peptone, and 100 mL of distilled artificial seawater) and incubating at 28 °C for 35 days under static conditions.

4.3. Extraction and isolation

After 35 days of fermentation, the rice medium (90 kg) of *Aspergillus* sp. EGF 15-0-3 was soaked and extracted with EtOAc three times (8 h per time) and evaporated under reduced pressure to afford the EtOAc extracts (900 g). The residue was then subjected to silica gel column eluted with a gradient of PE/EtOAc (100∶0–0∶100) to afford 8 major fractions (Fr. A–Fr. H) by TLC and HPLC analyses. Fr. F (33.7715 g) was applied to MCI column chromatography (MeOH/H_2O, *V*/*V*, 20∶80–100∶0) to give 8 subfractions (Fr. F1–Fr. F8). Subfraction F8 then was eluted with CH_2Cl_2/MeOH (30∶70) on Sephadex LH-20 column chromatography to afford 10 subfractions (Fr. F8-1–Fr. F8-10). Subfraction F8-6 (0.7410 g) was further separated repeatedly using preparative HPLC with 75% aqueous MeOH (flow rate of 3.0 mL·min^{-1}) to yield compound **2** (t_R = 43.27 min, 6.0 mg) and **5** (t_R = 57.32 min, 4.0 mg). Subfraction F8-7 (1.7816 g) was purified by repeated semipreparative HPLC with aqueous MeOH (MeOH/H_2O, *V*/*V*, 75∶25, flow rate of 3.0 mL·min^{-1}) to yield compounds **6** (t_R = 64.16 min, 4.0 mg), **7** (t_R = 52.24 min, 10.0 mg) and **8** (t_R = 68.73 min, 6.0 mg); subfraction F8-8 (2.5546 g) was applied to repeated semipreparative HPLC with aqueous MeOH or MeCN (flow rate of 3.0 mL·min^{-1}) to yield **1** (t_R = 42.33 min, 4.0 mg) and **4** (t_R = 58.12 min, 4.0 mg) ; and subfraction F8-9 (1.9987 g) was purified by repeated semipreparative HPLC with reverse-phase eluent (MeOH/H_2O, *V*/*V*, 70∶30) and the normal-phase eluent ($V_{isopropanol}$∶$V_{n\text{-}hexane}$ = 10∶90) to afford **3** (t_R =

Table 2 ^{1}H NMR (400 MHz) and ^{13}C NMR (100 MHz) data of **4**–**6** in DMSO-d_6 (J in Hz)[a].

No.	**4**		**5**		**6**	
	δ_H (J, Hz)	δ_C, type	δ_H (J, Hz)	δ_C, type	δ_H (J, Hz)	δ_C, type
1	11.02 (s)		11.10 (s)		11.12 (s)	
2		145.5, C		145.1, C		144.8, C
3		104.3, C		104.2, C		103.9, C
3a		126.5, C		126.3, C		126.4, C
4	7.01 (s)	119.2, CH	7.18 (d, 8.0)	119.1, CH	7.45 (d, 8.0)	119.5, CH
5		132.4, C	7.01 (d, 8.0)	119.5, CH	7.04 (t, 8.0)	119.4, CH
6	6.89 (dd, 8.0, 1.6)	121.5, CH	7.09 (d, 8.0)	120.8, CH	7.13 (t, 8.0)	120.8, CH
7	7.34 (d, 8.0)	111.7, CH	7.43 (d, 8.0)	111.8, CH	7.45 (d, 8.0)	111.6, CH
7a		133.7, C		135.1, C		135.2, C
8	6.97(s)	113.7, CH	7.00 (s)	113.8, CH	7.10 (s)	114.3, CH
9		124.9, C		124.5, C		124.2, C
10		164.1, C		160.7, C		161.7, C
11					9.37 (s)	
12		67.0, C		65.9, C		82.5, C
13		168.1, C		167.8, C		162.5, C
14	9.65 (s)		9.41 (s)		9.83 (s)	
15		39.2, C		39.0, C		39.0, C
16	6.03 (dd, 17.2, 10.4)	145.0, CH	6.03 (dd, 10.4, 17.2)	145.0, CH	6.11 (dd, 17.2, 10.4)	145.1, CH
17	a 5.01 (dd, 13.2, 1.2)	112.0, CH_2	a 5.00 (m)	111.9, CH_2	a 5.06 (dd, 17.6, 1.2)	111.8, CH_2
	b 5.04 (dd, 8.2, 1.2)		b 5.03 (m)		b 5.09 (dd, 10.4, 1.2)	
18	1.48 (s)	27.7, CH_3	1.47 (s)	27.6, CH_3	1.52 (s)	27.9, CH_3
19	1.45 (s)	28.2, CH_3	1.41 (s)	28.0, CH_3	1.49 (s)	27.5, CH_3
20	a 2.07 (m)	37.8, CH_2	a 1.79 (dd, 12.8, 9.0)	38.2, CH_2	a 2.18	26.6, CH_2
	b 2.26 (m)[a]		b 2.19 (dd, 12.8, 9.0)		b 2.16	
21	a 2.30 (m)[a]	28.0, CH_2				
	b 3.18 (m)a					
22	5.26 (m)[a]	122.2, CH				
23		130.7, C				
24	1.65 (s)	17.8, CH_3				
25	1.67 (s)	25.6, CH_3				
1′		115.7, C		116.8, C		106.0, C
2′		150.2, C		142.7, C		153.4, C
3′		123.0, C		122.1, C		129.4, C
4′	6.62 (s)	119.6, CH	6.60 (s)	114.3, CH	6.93 (s)	123.9, CH
5′		145.2, C		150.5, C		141.0, C
6′		131.1, C		121.6, C		119.4, C
7′	4.91 (d, 2.8)	54.7, CH	4.55 (d, 2.4)	51.4, CH	3.66 (td, 11.6, 6.4)	27.4, CH
8′	4.34 (dd, 4.0, 2.8)	68.4, CH	4.17 (d, 2.4)	72.9, CH	4.53 (t, 11.6)	83.9, CH
9′	3.21 (m)	42.0, CH	3.32 (m)[a]	44.5, CH	a 1.71 (m)	31.1, CH_2
					b 1.83 (m)	
10′	5.77 (m)[a]	122.4, CH	5.77 (m)	124.7, CH	a 1.44 (m)	23.4, CH_2
					b 1.61 (m)	
11′	5.75 (m)[a]	133.9, CH	5.75 (m)	135.1, CH	1.34 (m)	31.0, CH_2
12′	2.30 (m)[a]	28.2, CH	2.30 (t, 12.8)	26.5, CH	1.34 (m)	22.1, CH_2
13′	1.06 (d, 6.8)	20.5, CH_3	1.13 (d, 6.4)	19.9, CH_3	0.90 (t, 6.4)	14.0, CH_3
14′	5.66 (s)	94.1, CH	5.42 (s)	95.1, CH		169.1, C
15′	3.27 (m)[a]	34.7, CH_2	5.78 (d, 9.8)	121.6, CH	3.26 (d, 7.6)	27.1, CH_2
16′	5.26 (m)[a]	124.9, CH	6.36 (d, 9.8)	132.4, CH	5.25 (t, 7.6)	121.4, CH
17′		131.9, C		75.5, C		132.9, C
18′	1.71 (s)	17.8, CH_3	1.36 (s)	27.7, CH_3	1.66 (s)	17.6, CH_3
19′	1.68 (s)	25.6, CH_3	1.29 (s)	26.9, CH_3	1.65 (s)	25.4, CH_3
20′	3.36 (s)	54.8, CH_3	3.46 (s)	55.9, CH_3		
2′-OH	9.31 (s)				10.61 (s)	
5′-OH	7.89 (s)		8.95 (s)			

[a] Overlapped signals are reported without designating multiplicity.

Table 3 ^{1}H NMR (400 MHz) and ^{13}C NMR (100 MHz) data of **7**–**8** in DMSO-d_6 (δ in ppm, J in Hz)[a].

No.	7		8	
	δ_H (J, Hz)	δ_C, type	δ_H (J, Hz)	δ_C, type
1	11.18 (s)		10.98 (s)	
2		144.4, C		144.6, C
3		103.6, C		103.4, C
3a		126.3, C		126.3, C
4	7.14 (dd, 8.0, 1.0)	119.0, CH	7.50 (d, 1.0)	118.9, CH
5	7.09 (t, 8.0)	119.5, CH		132.7, C
6	7.03 (t, 8.0)	120.8, CH	6.93 (dd, 8.0, 1.0)	121.7, CH
7	7.44 (dd, 8.0, 1.0)	112.5, CH	7.33 (d, 8.0)	111.5, CH
7a		132.8, C		133.6, C
8	6.90 (s)	111.0, CH	6.91 (s)	111.3, CH
9		123.9, C		123.9, C
10		167.3, C		167.3, C
11	7.55 (s)		7.75 (s)	
12		59.3, C		59.2, C
13		160.7, C		161.0, C
14	8.87 (s)		8.89 (s)	
15		39.0, C		39.0, C
16	6.05 (dd, 17.2, 10.4)	145.1, CH	6.05 (dd, 17.2, 10.4)	145.1, CH
17	a 5.00 (m) b 5.04 (m)	111.7, CH_2	a 5.00 (m) b 5.04 (m)	111.6, CH_2
18	1.45 (s)	27.6, CH_3	1.44 (s)	27.6, CH_3
19	1.45 (s)	27.5, CH_3	1.44 (s)	27.6, CH_3
20	a 1.76 (dd, 13.6, 7.2) b 2.16 (dd, 13.6, 7.2)	37.5, CH_2	a 1.75 (dd, 13.4, 7.0) b 2.26 (m)[a]	37.4, CH_2
21			3.32 (d, 7.0)	34.3, CH_2
22			5.28 (dd, 7.0, 1.6)	121.4, CH
23				132.3, C
24			1.62 (s)	25.5, CH_3
25			1.60 (s)	17.6, CH_3
1′		112.5, C		112.5, C
2′		158.9, C		158.6, C
3′		126.1, C		130.6, C
4′	7.56 (s)	118.8, CH	7.03(s)	118.1, CH
5′		148.7, C		148.5, C
6′		126.9, C		126.7, C
7′	7.21 (s)	104.7, CH	7.19 (s)	104.8, CH
8′		156.3, C		157.0, C
9′	4.20 (dt, 4.0, 2.0)	42.7, CH	4.20 (dt, 4.0, 2.0)	45.6, CH
10′	5.77 (ddd, 10.0, 4.0, 2.4)	121.6, CH	5.74 (ddd, 10.0, 4.0, 2.4)	121.6, CH
11′	5.93 (dt, 10.0, 2.4)	134.7, CH	5.92 (dt, 10.0, 2.4)	134.7, CH
12′	2.81 (m)	28.4, CH	2.83 (m)	28.5, CH
13′	1.18 (d, 7.2)	21.2, CH_3	1.17 (d, 7.2)	21.1, CH_3
14′	10.44 (s)	193.9, CH	10.42 (s)	193.7, CH
15′	3.30 (d, 7.2)	27.5, CH_2	3.30 (d, 7.2)	27.5, CH_2
16′	5.28 (dd, 7.2, 1.6)	121.6, CH	5.28 (dd, 7.2, 1.6)	124.5, CH
17′		135.1, C		135.5, C
18′	1.65 (s)	17.6, CH_3	1.64 (s)	17.6, CH_3
19′	1.63 (s)	25.5, CH_3	1.63 (s)	25.6, CH_3
2′-OH	11.17 (s)			
5′-OH				

[a] Overlapped signals are reported without designating multiplicity.

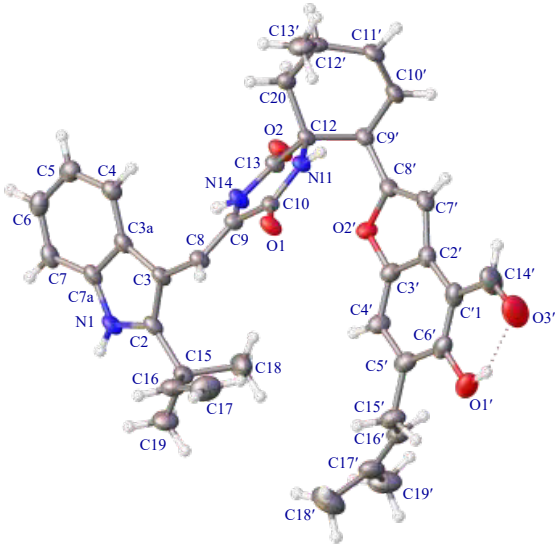

Fig. 4 ORTEP drawing of compound **7**.

28.26 min, 4.0 mg).

*4.4. Structural characterizations of **1**–**8***

(±)-Aspergilline E (**1**): red brown powder (MeOH), $[\alpha]_D^{20}$ ± 0 (c 0.10, MeOH); UV (MeOH) λ_{max} (log ε): 226 (1.58), 269 (0.47), 339 (0.41) nm; IR (KBr) ν_{max}: 3354, 3024, 2966, 2926, 1685, 1608, 1473, 1456, 1423, 1139, 925, 748 cm^{-1}; HR-ESI-MS (ESI-TOF) m/z: [M + H]$^+$ 648.3073 (Calcd. for $C_{39}H_{42}N_3O_6$ 648.3074); ^{1}H NMR (400 MHz, DMSO-d_6) and ^{13}C NMR (100 MHz, DMSO-d_6) see Table 1.

(+)-**1**: $[\alpha]_D^{20}$ +47.16 (c 0.05, MeOH); CD (MeOH) λ_{max} ($\Delta\varepsilon$): 208 (44.44), 277 (−17.44), 374 (1.63). (−)-**1**: $[\alpha]_D^{20}$ −47.73 (c 0.05, MeOH); CD (MeOH) λ_{max} ($\Delta\varepsilon$): 207 (−39.96), 278 (18.98), 374 (−1.55).

(±)-Aspergilline F (**2**): red brown powder (MeOH), $[\alpha]_D^{20}$ ±0 (c 0.10, MeOH); UV (MeOH) λ_{max} (log ε): 223 (0.70), 269 (0.17), 340 (0.18) nm; IR (KBr) ν_{max}: 3365, 3309, 3024, 2962, 2918, 1685, 1606, 1473, 1456, 1423, 1139, 1051, 748 cm^{-1}; HR-ESI-MS (ESI-TOF) m/z: [M + H]$^+$ 648.3074 (Calcd. for $C_{39}H_{42}N_3O_6$ 648.3074); ^{1}H NMR (400 MHz, DMSO-d_6) and ^{13}C NMR (100 MHz, DMSO-d_6) see Table 1.

(+)-**2**: $[\alpha]_D^{20}$ +46.17 (c 0.05, MeOH); CD (MeOH) λ_{max} ($\Delta\varepsilon$): 215 (−36.37), 244 (−70.09), 289 (−35.26), 353 (64.88). (−)-**2**: $[\alpha]_D^{20}$ −45.95 (c 0.05, MeOH); CD (MeOH) λ_{max} ($\Delta\varepsilon$): 215 (50.73), 242 (65.87), 289 (24.38), 354 (−59.62).

(±)-Aspergilline G (**3**): yellow powder (MeOH), $[\alpha]_D^{20}$ ±0 (c 0.10, MeOH); UV (MeOH) λ_{max} (log ε): 224 (0.70), 264 (0.17), 343 (0.18) nm; IR (KBr) ν_{max}: 3346, 3255, 2966, 2908, 1670, 1456, 1423, 1139, 1083, 721 cm^{-1}; HR-ESI-MS (ESI-TOF) m/z: [M + H]$^+$ 634.2899 (Calcd. for $C_{38}H_{40}N_3O_6$ 634.2917); ^{1}H NMR (400 MHz, DMSO-d_6) and ^{13}C NMR (100 MHz, DMSO-d_6) see Table 1.

(+)-**3**: $[\alpha]_D^{20}$ +40.02 (c 0.05, MeOH); CD (MeOH) λ_{max} ($\Delta\varepsilon$): 223 (−51.19), 256 (−29.64), 304 (8.31). (−)-**3**: $[\alpha]_D^{20}$ −43.21 (c 0.05, MeOH); CD (MeOH) λ_{max} ($\Delta\varepsilon$): 224 (46.59), 253 (28.29), 289, 354 (−7.91).

(±)-Aspergilline H (**4**): light yellow powder (MeOH), $[\alpha]_D^{20}$ ±0 (c 0.10, MeOH); UV (MeOH) λ_{max} (log ε): 222 (1.07), 269 (0.34), 338 (0.18) nm; IR (KBr) ν_{max}: 3354, 2962, 2929, 2872, 1687, 1660, 1471, 1425, 1184, 925, 740, 544 cm^{-1}; HR-ESI-MS (ESI-TOF) m/z: [M + H]$^+$ 718.3846 (Calcd. for $C_{44}H_{52}N_3O_6$ 718.3856); ^{1}H NMR (400 MHz, DMSO-d_6) and ^{13}C NMR (100 MHz, DMSO-d_6) see Table 2.

(+)-**4**: $[\alpha]_D^{20}$ +52.20 (c 0.05, MeOH); CD (MeOH) λ_{max} ($\Delta\varepsilon$): 213

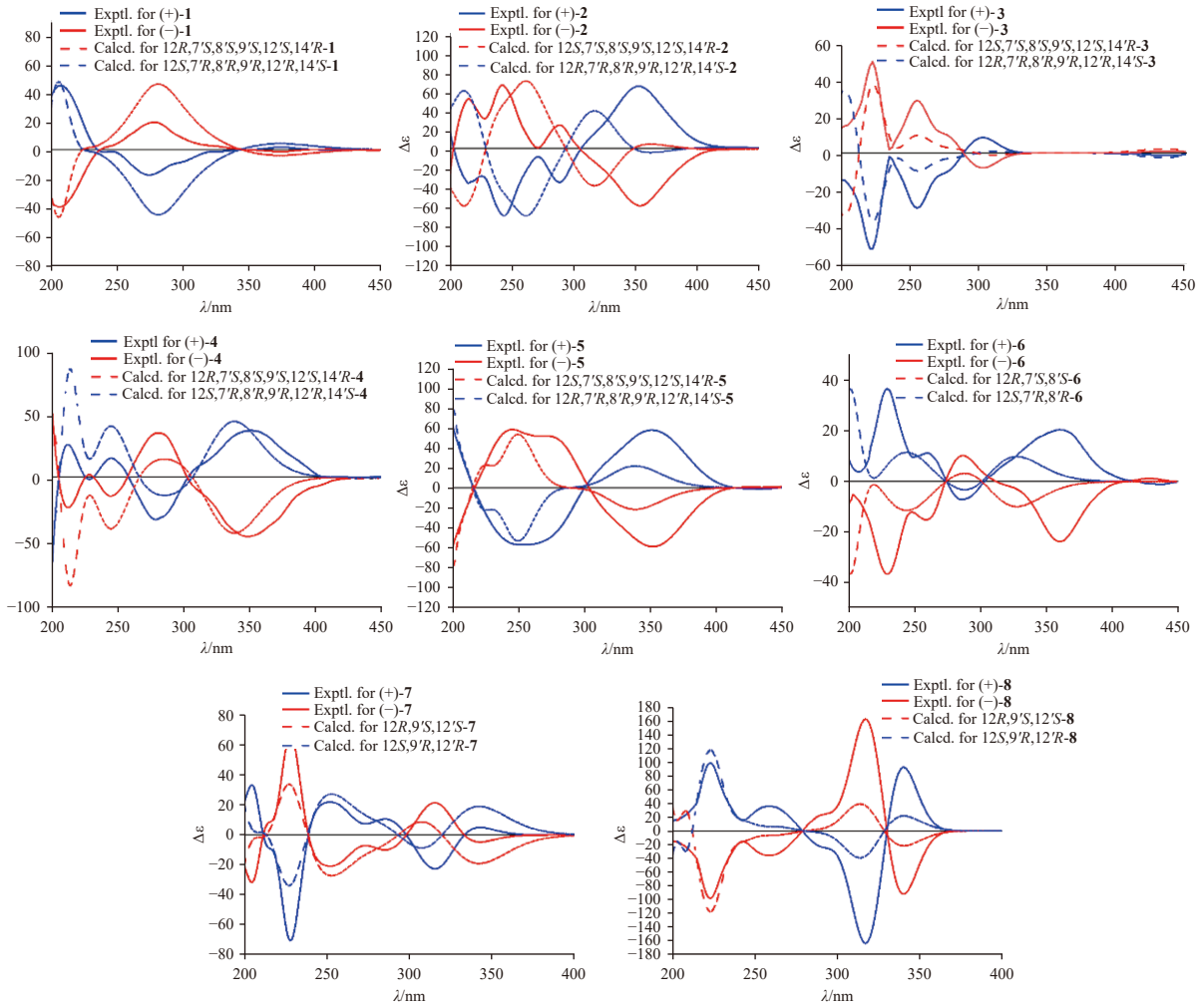

Fig. 5 Experimental and calculated ECD spectra of (+)-**1**, (−)-**1**, (+)-**2**, (−)-**2**, (+)-**3**, (−)-**3**, (+)-**4**, (−)-**4**, (+)-**5**, (−)-**5**, (+)-**6**, (−)-**6**, (+)-**7**, (−)-**7**, (+)-**8**, and (−)-**8**.

Table 4 TDP2 inhibitory activities of compounds **1**–**8**[a].

Compounds	IC_{50}/(μmol·L^{-1})	Compounds	IC_{50}/(μmol·L^{-1})
1	37.22 ± 1.94	**6**	11.10 ± 2.40
2	9.10 ± 1.00	**7**	10.30 ± 1.20
3	11.80 ± 2.40	**8**	16.90 ± 7.80
4	69.12 ± 3.81	YH-F83	0.46 ± 0.15
5	17.50 ± 2.50		

[a]All data were presented as means ± SD of at least three independent experiments.

(25.66), 246 (14.79), 279 (−32.96), 351 (36.48). (−)-**4**: $[\alpha]_D^{20}$ −51.55 (*c* 0.05, MeOH); CD (MeOH) λ_{max} (Δε): 213 (−23.84), 245 (−14.61), 281 (34.57), 350 (−46.34).

(±)-Aspergilline I (**5**): light yellow powder (MeOH), $[\alpha]_D^{20}$ ±0 (*c* 0.10, MeOH); UV (MeOH) λ_{max} (log ε): 224 (1.32), 264 (0.38), 346 (0.41) nm; IR (KBr) ν_{max}: 3367, 3215, 2960, 2929, 1689, 1653, 1624, 1456, 1394, 1186, 923, 742, 540 cm^{-1}; HR-ESI-MS (ESI-TOF) *m/z*: [M + H]$^+$ 648.3075 (Calcd. for $C_{39}H_{42}N_3O_6$ 648.3074) ; ^{1}H NMR (400 MHz, DMSO-d_6) and ^{13}C NMR (100 MHz, DMSO-d_6) see Table 2.

(+)-**5**: $[\alpha]_D^{20}$ +51.47 (*c* 0.05, MeOH); CD (MeOH) λ_{max} (Δε): 255 (−56.91), 352 (57.38). (−)-**5** $[\alpha]_D^{20}$ −51.55 (*c* 0.05, MeOH); CD (MeOH) λ_{max} (Δε): 247 (58.00), 353 (-58.69).

(±)-Aspergilline J (**6**): light yellow powder (MeOH), $[\alpha]_D^{20}$ ±0 (*c* 0.10, MeOH); UV (MeOH) λ_{max} (log ε): 223 (1.29), 264 (0.42), 347 (0.38) nm; IR (KBr) ν_{max}: 3348, 3280, 2962, 2918, 1681, 1670, 1435, 1255, 920, 740 cm^{-1}; HR-ESI-MS (ESI-TOF) *m/z*: [M + H]$^+$ 638.3223 (Calcd. for $C_{38}H_{44}N_3O_6$ 638.3230); ^{1}H NMR (400 MHz, DMSO-d_6) and ^{13}C NMR (100 MHz, DMSO-d_6) see Table 2.

(+)-**6**: $[\alpha]_D^{20}$ +46.47 (*c* 0.05, MeOH); CD (MeOH) λ_{max} (Δε): 229 (36.44), 260 (11.15), 286 (−7.01), 360 (20.34). (−)-**6**: $[\alpha]_D^{20}$ −46.25 (*c* 0.05, MeOH); CD (MeOH) λ_{max} (Δε): 229 (−36.40), 258 (−15.04), 287 (10.13), 361 (−23.63).

(±)-Aspergilline K (**7**): yellow powder (MeOH), mp 137–138 °C, $[\alpha]_D^{20}$ ±0 (*c* 0.10, MeOH); UV (MeOH) λ_{max} (log ε): 219 (0.69), 279 (0.32), 339 (0.29) nm; IR (KBr) ν_{max}: 3558, 3192, 2958, 2926, 2854, 1697, 1670, 1653, 1456, 1219, 966, 742 cm^{-1}; HR-ESI-MS (ESI-TOF) *m/z*: [M + H]$^+$ 618.2964 (Calcd. for $C_{38}H_{40}N_3O_5$ 618.2968); ^{1}H NMR (400 MHz, DMSO-d_6) and ^{13}C NMR (100 MHz, DMSO-d_6) see Table 3.

(+)-**7**: $[\alpha]_D^{20}$ +115.80 (*c* 0.10, MeOH); CD (MeOH) λ_{max} (Δε): 205 (33.37), 228 (−70.43), 252 (21.91), 285 (10.60). (−)-**7**: $[\alpha]_D^{20}$ −113.95 (*c* 0.10, MeOH); CD (MeOH) λ_{max} (Δε): 215 (−31.10), 228 (66.79), 252 (−20.78), 286 (−10.05).

(±)-Aspergilline L (**8**): yellow brown powder (MeOH), $[\alpha]_D^{20}$ ±0 (*c* 0.10, MeOH); UV (MeOH) λ_{max} (log ε): 222 (0.71), 274 (0.30), 339 (0.28) nm; IR (KBr) ν_{max}: 3325, 3273, 2960, 2918, 2850, 1697, 1681, 1653, 1456, 1261, 972, 742 cm^{-1}; HR-ESI-MS (ESI-TOF) *m/z*: [M + H]$^+$ 686.3588 (Calcd. for $C_{43}H_{48}N_3O_5$ 686.3594); ^{1}H NMR (400 MHz, DMSO-d_6) and ^{13}C NMR (100 MHz, DMSO-d_6) see Table 3.

(+)-**8**: $[\alpha]_D^{20}$ +106.26 (*c* 0.05, MeOH); CD (MeOH) λ_{max} (Δε): 223 (98.98), 259 (38.88), 317 (−163.61), 340 (92.52). (−)-**8**: $[\alpha]_D^{20}$ −105.85 (*c* 0.05, MeOH); CD (MeOH) λ_{max} (Δε): 220 (−87.28), 260 (−35.56), 314 (151.64), 340 (−92.00).

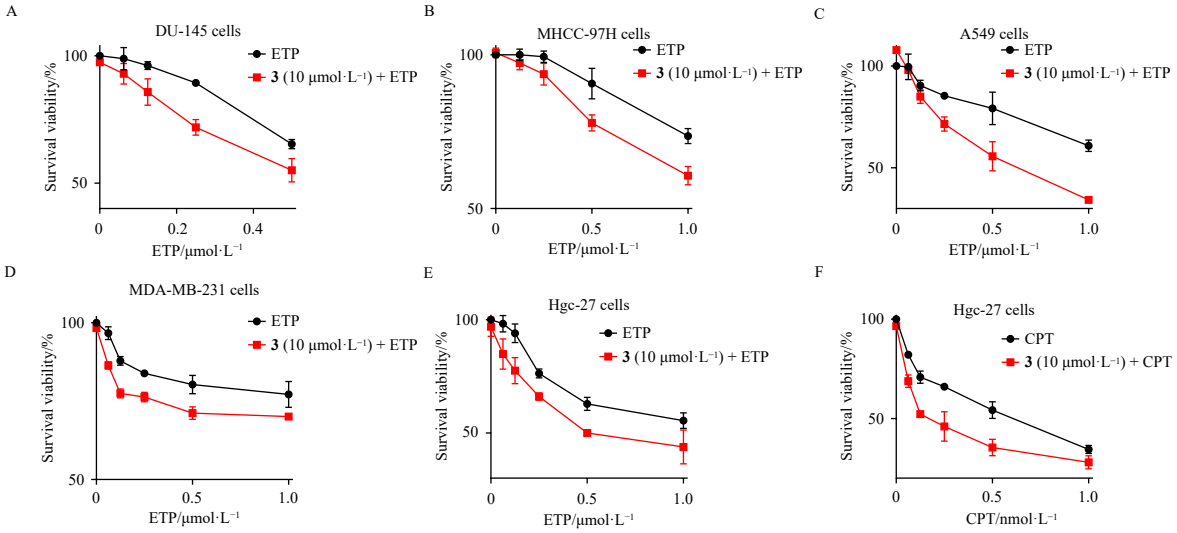

Fig. 6 Anti-tumor effects of compound **3**. (A–E) Synergistic effect of **3** with ETP in (A) DU-145, (B) MHCC-97, (C) A549, (D) MDA-MB-231, and (E) Hgc-27cell lines; (F) Synergistic effect of **3** with CPT in Hgc-27 cell lines. Data are presented as mean ± SD (n = 3).

*4.5. Chiral separation of compounds **1–8***

Compounds **1–8** were further separated using a chiral chromatographic column [FLM Chiral ND (2)] to obtain the optical pure enantiomers, respectively. More detailed information is included in the Supporting Information.

4.6. Electronic circular dichroism (ECD) calculations

The quantum chemical ECD calculations of **1–8** were performed according to modified protocols as reported previously [27]. Briefly, the random conformers searched by the SYBYL X 2.1.1 program using MMFF94s molecular force field, and an energy cutoff of 10 kcal·mol^{-1} to the global minima. The selective conformers were subsequently optimized by using Gaussion09 software at B3LYP/6-31 + G(d) level in methanol. No imaginary frequencies were found. The overall ECD data were all weighted by Boltzmann distribution and were subsequently compared with the experimental ones using SpecDis 1.70.1 software, respectively.

4.7. X-ray crystallographic analysis

Crystals of **7** was obtained by using the solvent vapor diffusion method in pure methanol. The intensity data of **7** was recorded on a Rigaku Oxford Diffraction Supernova diffractometer with Cu Kα radiation (λ = 1.541 84 Å). The crystal structure was solved and refined with the similar method reported previously [28-30]. Crystal data of **7** in the standard CIF format were deposited with the Cambridge Crystallographic Data Centre with CCDC numbers of 2353833.

Crystal data for **7**: $C_{38}H_{39}N_3O_5$, Mr = 617.72 g·mol^{-1}, triclinic, space group P-1, a = 10.0328(2) Å, b = 13.2598(2) Å, c = 14.3090(3) Å, Z = 2, T = 100.01(10) K, μ(Cu Kα) = 0.680 mm^{-1}, D_{calc} = 1.272 g·cm^{-3}, 56732 reflections measured (6.797° ≤ 2θ ≤ 145.758°), 6362 unique (R_{int} = 0.0409, R_{sigma} = 0.0188) which were used in all calculations. The final R_1 was 0.0394 [I > 2σ(I)] and wR_2 was 0.1045 (all data).

4.8. Cytotoxicity assay

Cell viability was evaluated by the CCK-8 assays according to the protocols as reported previously [31]. In brief, 3000 cells were seeded in 96-well plates and incubated for 24 h. Then, cells were treated with 50 and 100 μmol·L^{-1} concentrations of the tested compounds respectively in the growth medium for 72 h. After that, 10 μL of CCK-8 (Targetmol, USA) was added to every well followed by incubation for 90 min at 37 °C. The absorbance was subsequently measured using Synergy H4 Hybrid Microplate Reader (BioTek, Winooski, VT, USA) at 450 nm. The absorbance of cells treated with 0.1% DMSO was considered as 100% and the IC_{50} represents the concentration that inhibits cells proliferation by 50%. Each datum point is the mean ± SD of three independent experiments.

4.9. TDP2 inhibition assay

The TDP2 inhibition by the isolated compounds were performed through an oligonucleotide-based fluorescence assay, according to the method we had previously established [10]. Briefly, a quenched fluorescent single-stranded oligonucleotide was used as substrate. The compounds were tested at 100 μmol·L^{-1} concentration. Compounds that with notable TDP2 inhibition (> 50%) were further tested to investigate their TDP2 values.

Funding

This work was supported by the National Natural Science Foundation of China (Nos. 82273845, 82304331, 82360695, and 82173655) and Guangxi Natural Science Foundation Project (No. 2023GXNSFBA026236).

Supplementary data

Supplementary data for this study can be obtained by contacting the corresponding authors *via* E-mail.

Declaration of competing interest

These authors have no conflict of interest to declare.

Acknowledgment

This paper is dedicated to Profs. Longnei Zeng and Jingyu Su (School of Chemistry and Chemical Engineering, Sun Yat-Sen University) on the occasion of their 96th birthday.

References

1 Klausz K, Kellner C, Gehler CL, et al. The novel dual topoisomerase inhibitor P8-D6 shows anti-myeloma activity *in vitro* and *in vivo*. *Mol Cancer Ther*. 2022;21(1):70-78. https://doi.org/10.1158/1535-7163.MCT-21-0119.

2 Bondarev AD, Jonsson J, Chubarev VN, et al. Recent developments of topoisomerase inhibitors: clinical trials, emerging indications, novel molecules and global sales. *Pharmacol Res*. 2024;209:107431. https://doi.org/10.1016/j.phrs.2024.107431.

3 Talukdar A, Kundu B, Sarkar D, et al. Topoisomerase I inhibitors: challenges, progress and the road ahead. *Eur J Med Chem*. 2022;236:114304. https://doi.org/10.1016/j.ejmech.2022.114304.

4 Le TT, Wu M, Lee JH, et al. Etoposide promotes DNA loop trapping and barrier formation by topoisomerase II. *Nat Chem Biol*. 2023;19(5):641-650. https://doi.org/10.1038/s41589-022-01235-9.

5 Pype S, Declercq W, Ibrahimi A, et al. TTRAP, a novel protein that associates with CD40, tumor necrosis gactor (TNF) teceptor-75 and TNF receptor-sssociated gactors (TRAFs), and that inhibits nuclear factor-κB activation. *J Biol Chem*. 2000;275(24):18586-18593. https://doi.org/10.1074/jbc.M000531200.

6 Zhang JQ, Liang ZQ, Guo LS, et al. The oligonucleotide-based fluorescence assay for the discovery of tyrosyl-DNA phosphodiesterase 2 inhibitors. *Dyes Pigments*. 2024;227:112173. https://doi.org/10.1016/j.dyepig.2024.112173.

7 Shimizu N, Hamada Y, Morozumi R, et al. Repair of topoisomerase 1-induced DNA damage by tyrosyl-DNA phosphodiesterase 2 (TDP2) is dependent on its magnesium binding. *J Biol Chem*. 2023;299:104988. https://doi.org/10.1016/j.jbc.2023.104988.

8 Tsuda M, Kitamasu K, Kumagai C, et al. Tyrosyl-DNA phosphodiesterase 2 (TDP2) repairs topoisomerase 1 DNA-protein crosslinks and 3′-blocking lesions in the absence of tyrosyl-DNA phosphodiesterase 1 (TDP1). *DNA Repair*. 2020;91-92:102849. https://doi.org/10.1016/j.dnarep.2020.102849.

9 Zeng Z, Sharma A, Ju L, et al. TDP2 promotes repair of topoisomerase I-mediated DNA damage in the absence of TDP1. *Nucleic Acids Res*. 2012;40(17):8371-8380. https://doi.org/10.1093/nar/gks622.

10 Maede Y, Shimizu H, Fukushima T, et al. Differential and common DNA repair pathways for topoisomerase I- and II-targeted drugs in a genetic DT40 repair cell screen panel. *Mol Cancer Ther*. 2014;13(1):214-220. https://doi.org/10.1158/1535-7163.MCT-13-0551.

11 Siro G, Pipite A. Mini-review on the antimicrobial potential of actinobacteria associated with seagrasses. *Explor Drug Sci*. 2024;2:117-125. https://doi.org/10.37349/eds.2024.00038.

12 Ghareeb MA, Tammam MA, El-Demerdash A, et al. Insights about clinically approved and preclinically investigated marine natural products. *Curr Res Biotechnol*. 2020;2(11):88-102. https://doi.org/10.1016/j.crbiot.2020.09.001.

13 Francesch AM, Glaser KB, Jaspars M, et al. Pharmaceuticals from marine dources: past, present and future. *Pharm J*. 2024;312:15. https://doi.org/10.1211/PJ.2024.1.324083.

14 Karthikeyan A, Joseph A, Nair BG. Promising bioactive compounds from the marine environment and their ptential effects on various diseases. *J Genet Eng Biotechnol*. 2022;20:14. https://doi.org/10.1186/s43141-021-00290-4.

15 Ameen F, AlNadhari S, Al-Homaidan AA. Marine microorganisms as an untapped source of bioactive compounds. *Saudi J Biol Sci*. 2021;28(1):224-231. https://doi.org/10.1016/j.sjbs.2020.09.052.

16 Caesar LK, Butun FA, Robey MT, et al. Correlative metabologenomics of 110 fungi reveals metabolite-gene cluster pairs. *Nat Chem Biol*. 2023;19(7):846-854. https://doi.org/10.1038/s41589-023-01276-8.

17 Scherlach K, Hertweck C. Mining and unearthing hidden biosynthetic potential. *Nat Commun*. 2021;12:3864. https://doi.org/10.1038/s41467-021-24133-5.

18 Carroll AR, Copp BR, Grkovic T, et al. Marine natural products. *Nat Prod Rep*. 2025;42(2):257-297. https://doi.org/10.1039/D4NP00067F.

19 Dinglasan JLN, Otani H, Doering DT, et al. Microbial secondary metabolites: advancements to accelerate discovery towards application. *Nat Rev Microbiol*. 2025;23(6):338-354. https://doi.org/10.1038/s41579-024-01141-y.

20 Fan H, Shao XH, Wu PP, et al. Exploring brominated aromatic butenolides from *Aspergillus terreus* EGF7-0-1 with their antifungal activities. *J Agric Food Chem*. 2024;72(36):19869-19882. https://doi.org/10.1021/acs.jafc.4c04728.

21 Wei X, Wang FT, Si-Tu MX, et al. Pyranodipyran derivatives with tyrosyl DNA phosphodiesterase 1 inhibitory activities and fluorescent properties from *Aspergillus* sp. EGF 15-0-3. *Mar Drugs*. 2022;20(3):211. https://doi.org/10.3390/md20030211.

22 Wei X, Luo ZW, Zhang GQ, et al. Sterpiperazines A and B, steroid-indole alkaloids with Tdp1onhibitory and chemotherapy sensitizing activities from marine fungus *Aspergillus* sp. EGF 15-0-3. *Chin Chem Lett*. 2025;37(2):111048. https://doi.org/10.1016/j.cclet.2025.111048.

23 Fan H, Shi ZM, Lei YH, et al. Rare carbon-bridged citrinin dimers from the starfish-derived symbiotic fungus *Penicillium* sp. GGF16-1-2. *Mar Drugs*. 2022;20(7):443. https://doi.org/10.3390/md20070443.

24 Wie X, Su JC, Hu JS, et al. Probing indole diketopiperazine-based hybrids as environmental-induced products from *Aspergillus* sp. EGF 15-0-3. *Org Lett*. 2022;24(1):158-163. https://doi.org/10.1021/acs.orglett.1c03795.

25 Laev SS, Salakhutdinov NF, Lavrik OI. Tyrosyl-DNA phosphodiesterase inhibitors: progress and potential. *Bioorg Med Chem*. 2016;24(21):5017-5027. https://doi.org/10.1016/j.bmc.2016.09.045.

26 Barthelmes HU, Habermeyer M, Christensen MO, et al. TDP1 overexpression in human cells counteracts DNA damage mediated by topoisomerases I and II. *J Biol Chem*. 2004;279(53):55618-55625. https://doi.org/10.1074/jbc.M405042200.

27 Cai Q, Zha HJ, Yuan SY, et al. Diterpenoids from *Euphorbia fischeriana* with Kv1. 3 inhibitory activity. *J Nat Prod*. 2023;86(10):2379-2390. https://doi.org/10.1021/acs.jnatprod.3c00580.

28 Wu HR, Zhang CN, Dou BQ, et al. Identification of *O*-arylated huperzinines as novel cholinergic anti-inflammatory pathway agonists against gout arthritis. *Bioorg Chem*. 2024;152:107716. https://doi.org/10.1016/j.bioorg.2024.107716.

29 Yang J, Xiong XM, Gong LZ, et al. Diketopiperazines with anti-kin inflammation from marine-derived endophytic fungus *Aspergillus* sp. and configurational reassignment of aspertryptanthrins. *Chin J Nat Med*. 2025;23(8):980-989. https://doi.org/10.1016/S1875-5364(25)60933-2.

30 Tao B, Zhao XL, Shi ZY, et al. Discovery of bioactive polycyclic polyprenylated acylphloroglucinol from *Hypericum patulum* that protects against hepatic ischemia/reperfusion injury. *Chin J Nat Med*. 2025;23(9):1104-1110. https://doi.org/10.1016/S1875-5364(25)60975-7.

31 Zhang XR, Wang HW, Tang WL, et al. Discovery, synthesis, and evaluation of oxynitidine derivatives as dual inhibitors of DNA topoisomerase IB (TOP1) and tyrosyl-DNA phosphodiesterase 1 (TDP1), and potential antitumor agents. *J Med Chem*. 2018;61(22):9908-9930. https://doi.org/10.1021/acs.Jmedchem.8b00639.